

## Article

# The Corrosion Behaviors of an As-Rolled Mg-8Li (in wt.%) Alloy in Two Differently Concentrated NaCl Solutions

Baojie Wang <sup>1,\*</sup>, Jiyu Hou <sup>1</sup>, Jiyu Luan <sup>1</sup>, Daokui Xu <sup>2,\*</sup> , Haijing Sun <sup>1</sup> and Jie Sun <sup>1</sup>

<sup>1</sup> School of Environmental and Chemical Engineering, Shenyang Ligong University, Shenyang 110159, China; jyhou@126.com (J.H.); jyluan@126.com (J.L.); hjsun@sylu.edu.cn (H.S.); sunjie@sylu.edu.cn (J.S.)

<sup>2</sup> Key Laboratory of Nuclear Materials and Safety Assessment, Institute of Metal Research, Chinese Academy of Sciences, Shenyang 110016, China

\* Correspondence: bjwang@alum.imr.ac.cn (B.W.); dkxu@imr.ac.cn (D.X.)

**Abstract:** By means of an electrochemical workstation, hydrogen evolution device, optical microscope (OM) and scanning electron microscope (SEM), the corrosion behaviors of an as-rolled Mg-8%Li alloy with a dual phase structure in 0.9 wt.% NaCl and 3.5 wt.% NaCl solutions have been investigated and compared. The results show that when the immersion time exceeds 8 h, the hydrogen evolution rate of the alloy in the 0.9 wt.% NaCl is 3 times higher than that in the 3.5 wt.% NaCl solution. Moreover, the corrosion behaviors of the alloy are obviously different in the two differently concentrated NaCl solutions. In the 3.5 wt.% NaCl solution, the localized corrosion is much more severe and can occur simultaneously in the interior of both the  $\alpha$ -Mg and  $\beta$ -Li matrix phases. However, the localized corrosion in the 0.9 wt.% NaCl solution is obviously weak and mainly occurs at the  $\alpha$ -Mg phase.

**Keywords:** magnesium–lithium alloy; microstructure; localized corrosion; corrosion product film



**Citation:** Wang, B.; Hou, J.; Luan, J.; Xu, D.; Sun, H.; Sun, J. The Corrosion Behaviors of an As-Rolled Mg-8Li (in wt.%) Alloy in Two Differently Concentrated NaCl Solutions. *Coatings* **2022**, *12*, 406. <https://doi.org/10.3390/coatings12030406>

Academic Editor: Stefanos M. Skolianos

Received: 24 February 2022

Accepted: 17 March 2022

Published: 18 March 2022

**Publisher's Note:** MDPI stays neutral with regard to jurisdictional claims in published maps and institutional affiliations.



**Copyright:** © 2022 by the authors. Licensee MDPI, Basel, Switzerland. This article is an open access article distributed under the terms and conditions of the Creative Commons Attribution (CC BY) license (<https://creativecommons.org/licenses/by/4.0/>).

## 1. Introduction

Magnesium–lithium (Mg–Li) alloys are the lightest metallic materials known and their density is between 1.35–1.65 g/cm<sup>3</sup>, which is only 1/2 of that of aluminum alloys. Compared with traditional magnesium alloys, Mg–Li alloys have great application prospects in the fields of automotive, aerospace and the military due to their excellent deformation capacity, specific strength and stiffness [1–5]. Generally, the microstructure of Mg–Li alloys varies with the added Li content. The dual phase Mg–Li alloys is comprised of the  $\alpha$ -Mg phase and  $\beta$ -Li phase when the Li content is less than 10.3 wt.% and higher than 5.5 wt.% [5]. It has been widely reported that the duplex structured Mg–Li alloys exhibit a good combination of mechanical strength and plasticity [6–12], ensuring their wide application prospects compared to other Mg alloys. However, micro galvanic corrosion can easily occur between these two phases because the electrode potential of the  $\beta$ -Li phase is lower than that of the  $\alpha$ -Mg phase, resulting in the poor corrosion resistance of dual phase Mg–Li alloys [3,13–17].

Since the chloride ion (Cl<sup>−</sup>) is an aggressive ion and has strong activity, the corrosion behavior of magnesium alloys is generally reported to be positively correlated with chloride ion concentration [18–20]. It has been reported that the corrosion severity of uncoated and coated AZ31 samples was significantly increased with the concentration of chloride ions [20]. In the research of the corrosion behavior of AZ31D magnesium alloys in NaCl solutions, Shan et al. reported that due to the increased concentration of chloride ions, the high frequency capacitive loop shrank, and the open circuit potential shifted to a more negative direction [19]. However, it is also reported that the induced pitting corrosion in the simulated acid rain solutions was not sensitive to the chloride ion concentrations, but due to the AlMn phases, it was located at the grain boundary [21]. Accordingly, it can be concluded that the corrosion behavior of Mg alloys in NaCl solutions depends on the Cl<sup>−</sup> concentration and the microstructural characteristics. For Mg–Li based alloys, although

their corrosion behaviors in NaCl solutions have been widely reported [22–27], no related work about the effect of  $\text{Cl}^-$  concentrations on the corrosion behavior of Mg–Li alloys has been performed.

Previous work has demonstrated that severely localized corrosion was visible for the duplex structured Mg–Li alloy [28,29]. Based on the mechanism of pitting, the interior of the pits becomes acidic and acts as the filament tip, whilst the back end of the filament is alkaline and covered with corrosion products. The  $\text{OH}^-$  can respectively react with  $\text{Mg}^{2+}$  and  $\text{Li}^+$  to form  $\text{Mg}(\text{OH})_2$  and  $\text{LiOH}$ , and subsequently react with  $\text{CO}_2$  to produce  $\text{MgCO}_3$  and  $\text{Li}_2\text{CO}_3$  [3,5,29–31]. Xu et al. reported that a thin and dense outer layer of  $\text{Li}_2\text{CO}_3$  formed on the surface of the  $\beta$ -Li phase could effectively weaken the corrosion attack to the  $\beta$ -Li phase [30]. On the contrary, the porous and loose  $\text{MgCO}_3$  and  $\text{Mg}(\text{OH})_2$  formed on the surface of the  $\alpha$ -Mg phase can be easily destroyed by the  $\text{Cl}^-$  and then induce the initiation of pitting corrosion [3,5]. Based on the description mentioned above, it can be predicted that for the dual phase Mg–Li alloys, their corrosion resistance should be quite sensitive to the concentration of  $\text{Cl}^-$ . However, previous work seldomly focused on whether the concentration of  $\text{Cl}^-$  can influence the protectiveness of the corrosion product films to the  $\alpha$ -Mg and  $\beta$ -Li phase or not. Moreover, it is still unknown whether the concentration of  $\text{Cl}^-$  can change the corrosion mechanism of the dual-phase Mg–Li alloys.

In this work, through performing the hydrogen evolution test, corrosion morphology characterization and electrochemical experiments of an as-rolled dual phase Mg-8%Li alloy in different concentrated NaCl solutions, the target is to answer the following questions: (1) can the corrosion resistance of the alloy can be significantly influenced by the concentrations of chloride ions? (2) If yes, what is the difference of the corrosion mechanisms in different concentrated NaCl solutions? In addition, the corrosion process and corrosion mechanism of the alloy were deeply disclosed.

## 2. Materials and Methods

### 2.1. Sample Preparation

The experimental material used in this work is a typical ( $\alpha$ -Mg +  $\beta$ -Li) dual phase Mg-8%Li (in wt.%) alloy. Through the inductively coupled plasma atomic emission spectrum (ICP-AES) apparatus, its chemical composition was determined, as listed in Table 1. The alloy was prepared by melting the high purity Mg and Li bulks in a vacuum reaction furnace under the atmosphere of flux argon to avoid burning. After keeping for 40 min at 710 °C to homogenize it, the molten alloy was cast into plate ingots with a cross-section of 200 mm × 300 mm and a thickness of 50 mm. Then, thin plates with a cross-section of 150 mm × 150 mm and a thickness of 18 mm were cut from the ingot. After being homogenized at 300 °C for 30 min, the plates were rolled at room temperature and their thickness was controlled to be 6 mm. To eliminate the residual stress induced by the rolling process, plates were held at 300 °C for 1 h in an air furnace. Then, block samples with a dimension of 10 mm × 5 mm × 5 mm for electrochemical measurements were cut from the plates and mounted by the epoxy resin AB glue with an exposed working area of 5 mm × 10 mm. Then, samples were grinded gradually with 400#, 800#, 1000# and 2000# water abrasive papers to remove the surface scratches, followed by washing with acetone and drying with cold air. Moreover, samples for the immersion and hydrogen evolution tests were polished with 2.5  $\mu\text{m}$  diamond paste after grinding. To clearly reveal the microstructure of the alloy, the polished surface of one sample was etched by an etchant solution of (4%  $\text{HNO}_3$  + 96%  $\text{C}_2\text{H}_5\text{OH}$ ) and subsequently observed by using an optical microscope (OM). Based on the “ImageJ” software, the occupied area fractions of two matrix phases were measured.

**Table 1.** Chemical composition of Mg-8%Li alloy.

Chemical Composition	Li	Fe	Mg
Content (wt.%)	7.85	<0.001	balance

## 2.2. Electrochemical Tests

The CS350 electrochemical workstation (Corrtest Co. Ltd., Wuhan, China) was used for the electrochemical test. The traditional three-electrode set-up was applied, i.e., the exposed areas of the mounted samples were the working electrode, the saturated calomel electrode (SCE) was the reference electrode and the platinum plate was the auxiliary electrode. After being pre-immersed in 0.9 wt.% NaCl and 3.5 wt.% NaCl solutions, respectively, for 0, 4, 8 and 24 h, their electrochemical measurements are performed. Before the measurements of potentiodynamic polarization curves and electrochemical impedance spectrum, a delay of 10 min was required to obtain a stable open circuit potential. The scanning rate of potentiodynamic polarization measurements is 0.166 mV/s. Potentiodynamic polarization curves were fitted by CorrView software. Electrochemical impedance spectra (EIS) were measured in a frequency range from 100 kHz to 10 mHz with a disturbed potential amplitude of 10 mV and subsequently fitted by using the ZSimDemo 3.30 software. To reveal the deviation of the measured data, each electrochemical experiment was carried out at least three times. Finally, the electrochemical curves were drawn by Origin 2019 software.

## 2.3. Hydrogen Evolution Measurements and Immersion Test

It has been reported that when Mg alloys are exposed to the aqueous solutions, the hydrogen evolution reaction due to the cathodic reaction (i.e.,  $2\text{H}^+ + 2\text{e} \rightarrow \text{H}_2\uparrow$ ) could take place [32,33]. Thus, the measured volume of the evolved hydrogen is related to the anodic dissolution of the substrate of Mg alloys [32]. The schematic diagram of the hydrogen evolution device used in the current investigation is shown in Figure 1. The polished samples were respectively immersed into the 0.9 wt.% NaCl and 3.5 wt.% NaCl solutions. The ratio of the corrosion medium volume to the exposed area of samples was set to 200:1. The measurements of hydrogen evolution volume were performed up to 48 h and the data were recorded every 2 h. After being respectively immersed in 0.9 wt.% NaCl and 3.5 wt.% NaCl solution for 4, 8 and 24 h, the surface morphologies and their three-dimensional (3D) profiles were observed by using a stereo optical microscope (VHX-900F, Keyence International, Mechelen, Belgium). The operational principle for obtaining 3D images with precise changes in height includes two steps: (1) taking the image at the same location automatically layer by layer; (2) combining all images into one. Moreover, the cross-sectional morphologies of the immersed samples were observed by using a scanning electron microscope (SEM; FEI Quanta 450, Hillsboro, OR, USA).

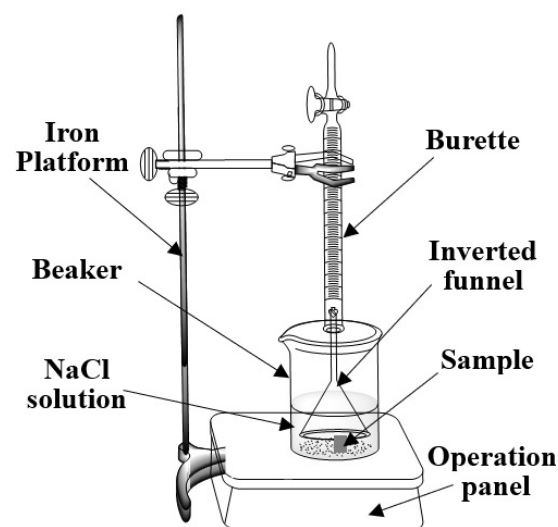
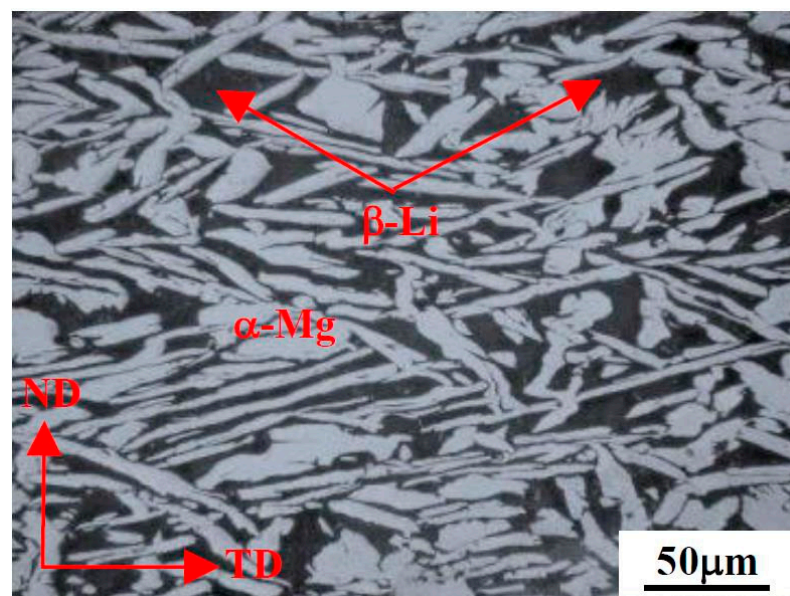


Figure 1. Schematic diagram of hydrogen evolution apparatus.

### 3. Results

#### 3.1. Microstructure

Figure 2 shows the optical microstructure of the as-rolled Mg-8%Li alloy. It can be seen that the alloy exhibits a typical dual phase structure. Generally, for the Mg–Li binary alloys, they are composed of  $\alpha$ -Mg and  $\beta$ -Li phases when the added Li content varies from 5.5 to 10.3 wt.% [3,5,10,14]. Moreover, for the duplex structured Mg–Li alloys, the  $\alpha$ -Mg and  $\beta$ -Li matrix phases respectively appear in white and black when observed by using OM [3,5,10,14]. Based on the Mg–Li binary phase diagram proposed by Masing et al. [34], the start melting temperature of  $\beta$ -Li phase is lower than that of the  $\alpha$ -Mg phase and decreases from 592 °C to 180.6 °C with the increase of Li content in the  $\beta$ -Li phase. Therefore, the  $\alpha$ -Mg phase first nucleates and grows at random sites during solidification process, resulting in their irregular and messy distribution. On the basis of the measurement from Image J software, the area fraction of the  $\alpha$ -Mg phase is determined to be 60%.



**Figure 2.** Optical microstructure of the as-rolled Mg-8%Li alloy.

#### 3.2. Electrochemical Responses

Figure 3 shows the potentiodynamic polarization curves of the samples being respectively pre-immersed in the two NaCl solutions for 0, 4, 8 and 24 h. It can be clearly seen that their cathodic branches are basically overlapped, indicating that the  $\text{Cl}^-$  concentration has almost no impact on the cathodic process. Since the negative difference effect and anodic dissolution occur during anodic polarization and then have a great impact on the sample surface, the cathodic and anodic branches of the polarization curves are asymmetric and the current density in the anodic section increases rapidly. As a result, the cathodic branch is generally used for fitting analysis [28]. The Tafel fitted results of potentiodynamic polarization curves are listed in Table 2. This reveals that the corrosion current densities of the samples being pre-immersed in the 0.9 wt.% NaCl are less than those being pre-immersed in the 3.5 wt.% NaCl. In addition, the corrosion potentials of the samples are much higher in the 0.9 wt.% NaCl than those in the 3.5 wt.% NaCl. After performing pre-immersion for up to 24 h, the corrosion current density of the sample in the 0.9 wt.% NaCl increased from the initial value of  $1.9735 \times 10^{-5}$  to  $5.104 \times 10^{-5}$  A/cm<sup>2</sup>. However, the current density of the sample in the 3.5 wt.% NaCl corrosion medium increased from the initial value of  $2.1679 \times 10^{-5}$  to  $6.1598 \times 10^{-5}$  A/cm<sup>2</sup>. Thus, the corrosion current density of samples in two concentrated solutions increases continuously with the prolongation of pre-immersion time. Moreover, the increased rate of corrosion current density of the samples due to the pre-immersion in the 3.5 wt.% NaCl is much higher than those in the

0.9 wt.% NaCl. Generally, the lower corrosion current density ensures the alloys have better corrosion resistance [35]. Compared with the corrosion in the 3.5 wt.% NaCl solution, samples immersed in the 0.9 wt.% NaCl have better corrosion resistance.

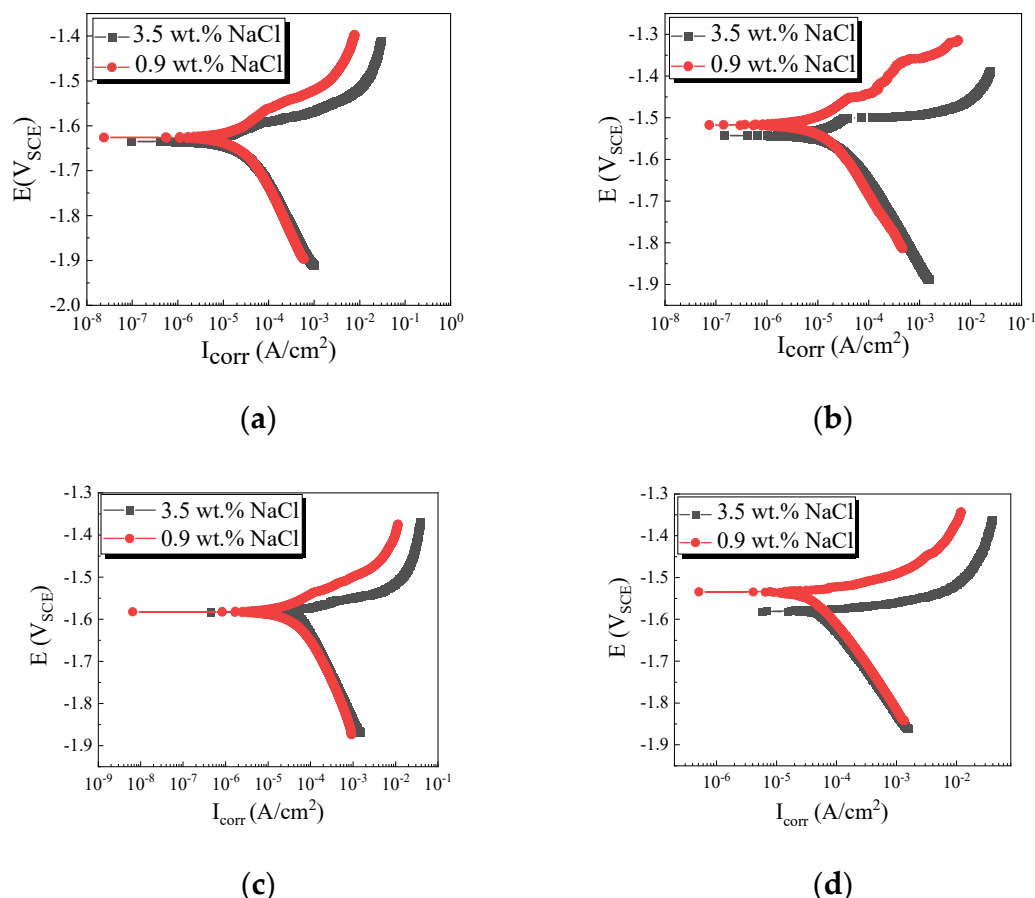


**Figure 3.** Potentiodynamic polarization curves of samples being pre-immersed in 0.9 wt.% NaCl and 3.5 wt.% NaCl solutions for different time: (a) 0 h, (b) 4 h, (c) 8 h and (d) 24 h.

**Table 2.** Fitted results of polarization curves.

Pre-Immersion Time	In 0.9 wt.% NaCl		In 3.5 wt.% NaCl	
	$E_{corr}$ (V <sub>SCE</sub> )	$i_{corr}$ (μA/cm <sup>2</sup> )	$E_{corr}$ (V <sub>SCE</sub> )	$i_{corr}$ (μA/cm <sup>2</sup> )
0 h	1.625 ± 0.005	20 ± 2	1.643 ± 0.005	22 ± 2
4 h	1.524 ± 0.003	24 ± 2	1.545 ± 0.003	43 ± 3
8 h	1.585 ± 0.003	41 ± 4	1.586 ± 0.003	55 ± 4
24 h	1.538 ± 0.003	51 ± 4	1.572 ± 0.003	62 ± 5

Figure 4 shows the AC impedance spectrum of the sample immersed in the 0.9 wt.% NaCl and 3.5 wt.% NaCl solutions for 0, 4, 8 and 24 h. For the samples measured in two concentrations of NaCl solutions, a high-frequency capacitive loop and a middle to low-frequency capacitive loop can be observed (Figure 4a). Moreover, the radius of the capacitive loop of the sample immersed in 3.5 wt.% NaCl is smaller than that in 0.9 wt.% NaCl. Generally, the larger the radius of the capacitive loop, the better the corrosion resistance of the sample [3,14,27,30]. Thus, the corrosion resistance of the sample immersed in 0.9 wt.% NaCl is much better. After being pre-immersed for 4 h, the impedance spectrum of the sample in 0.9 wt.% NaCl shows a high-frequency capacitive loop and a middle to low-frequency capacitive loop, whilst it contains a high frequency capacitive and a low-frequency inductive loop for the sample in the 3.5 wt.% NaCl solution (Figure 4b). Generally, the appearance of the low-frequency inductive loop indicates that the sample

surface is prone to pitting or localized corrosion [21]. Therefore, it indirectly reflects that the occurrence of pitting or localized corrosion may happen at the surface of the sample being immersed in the 3.5 wt.% NaCl solution for 4 h. After being pre-immersed for 8 h, the sample immersed in 0.9 wt.% NaCl contains a high-frequency capacitive loop, a middle to low-frequency capacitive loop and a low-frequency inductive loop, whilst the sample immersed in 3.5 wt.% NaCl contains a high-frequency capacitive and a low-frequency inductive loop (Figure 4c). Moreover, the radius of each of the capacitive loop of the two curves is reduced, demonstrating that the corrosion resistance decreases with increasing immersion time in both concentrated NaCl solutions. After being pre-immersed for 24 h, the AC impedance spectrums of the samples measured in two concentrated NaCl solutions contain a high frequency capacitive and a low-frequency inductive loop (Figure 4d). Moreover, the radius of their capacitive loops is further reduced. For the sample immersed in the 0.9 wt.% NaCl solution, the middle to low-frequency capacitive loop disappears. Based on the changes of the capacitive loop radius, this reflects that the corrosion resistance of the samples in the two NaCl solutions decreases further with the prolongation of immersion time. Additionally, the localized corrosion attack may occur earlier in the 3.5 wt.% NaCl solution, indicating that the corrosion resistance of the sample is much better in the 0.9 wt.% NaCl solution.

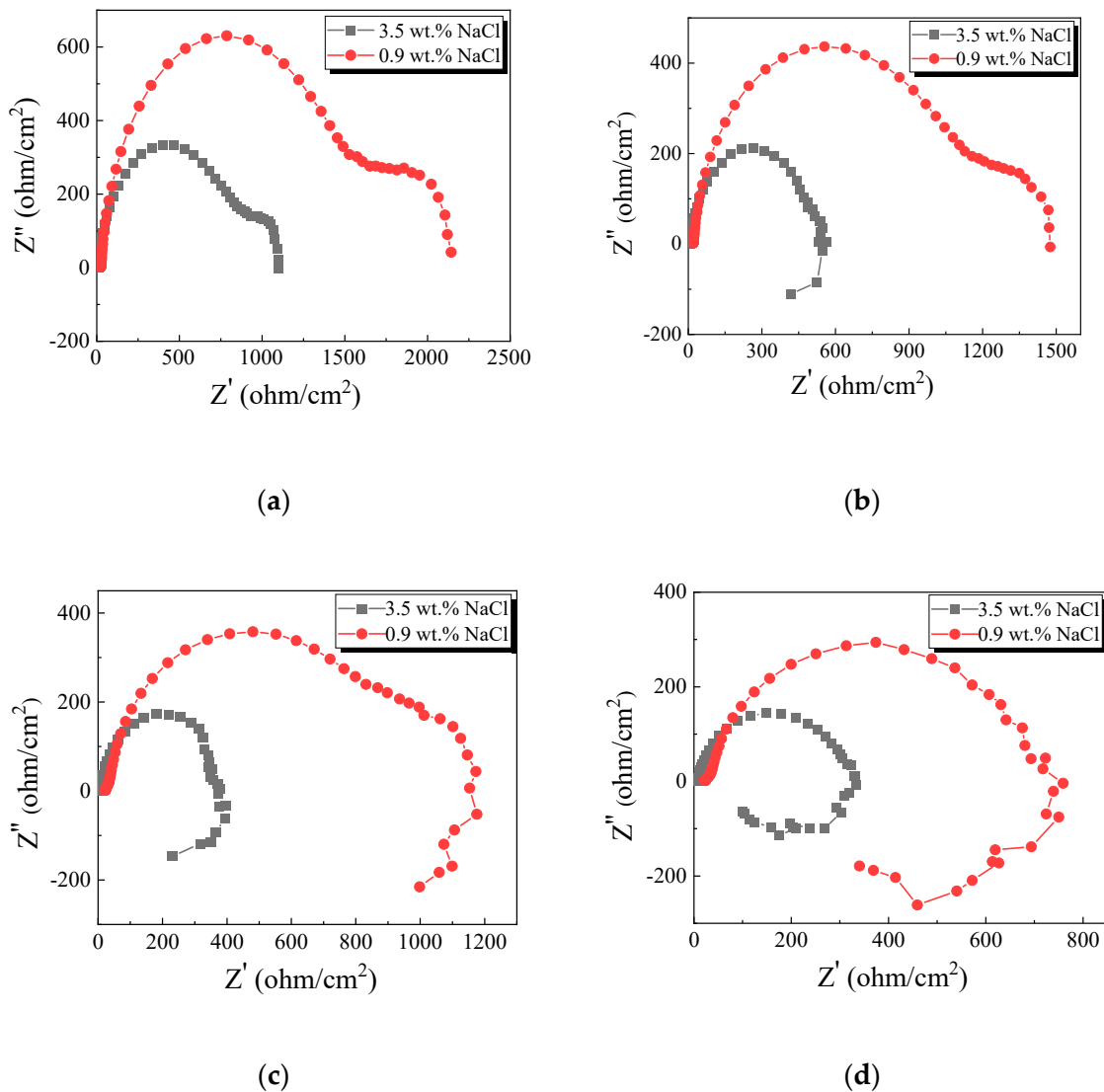


**Figure 4.** AC impedance spectrum of the Mg-8%Li alloy pre-immersed in 0.9 wt.% NaCl and 3.5 wt.% NaCl solution for different time: (a) 0 h, (b) 4 h, (c) 8 h and (d) 24 h.

To reflect the corrosion characteristics of the alloy being pre-immersed in two NaCl solutions for different times, electrochemical equivalent circuits were proposed to fit the EIS data, as shown in Figure 5. In the equivalent circuits,  $R_s$  is the solution resistance.  $R_{ct}$  and  $Q_{dl}$  represent charge transfer resistance and electric double layer, respectively, at the interface between substrate and electrolyte, which are used to describe the capacitance loop at high frequency.  $Q_{dl}$  is a constant phase element that replaces an ideal capacitor to account for the non-homogeneity in the system, which is defined by the two values of  $Y_{dl}$  and  $n_{dl}$ . Among them,  $n_{dl}$  is the dispersion coefficient of  $Q_{dl}$ . If  $n_{dl} = 1$ ,  $Q_{dl}$  is identical to a capacitor; if  $n_{dl} = 0$ ,  $Q_{dl}$  represents a resistance.  $R_f$  and  $Q_f$  (defined by  $Y_f$  and  $n_f$ ) represent film resistance and capacity in the medium frequency capacitance loop, respectively.  $R_L$  and  $L$  stand for resistance and inductance, respectively, which are used to describe the low frequency inductance loop and related to the localized corrosion [36].

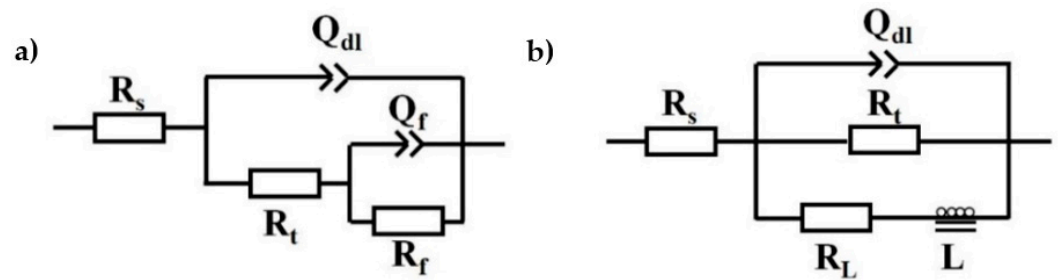


**Figure 5.** Equivalent circuits for the Mg-8%Li alloy pre-immersed in different NaCl solutions for different time: (a) 0 h and 4 h in 0.9 wt.% NaCl solution, 0 h in 3.5 wt.% NaCl solution, (b) 8 h and 24 h in 0.9 wt.% NaCl solution, 4 h, 8 h and 24 h in 3.5 wt.% NaCl solution.

The fitted results are listed in Table 3. It reveals that for the samples measured in two differently concentrated NaCl solutions, their  $R_{ct}$  values decrease with the prolongation of pre-immersed time. Moreover, the  $R_{ct}$  values measured in the 3.5 wt.% NaCl solution are obviously lower than those in the 0.9 wt.% NaCl solution. Thus, the corrosion resistance of the Mg-8%Li alloy in the 0.9 wt.% NaCl solution is relatively higher and decreases with the prolongation of pre-immersed time. In addition, the low frequency inductance loop in the 3.5 wt.% NaCl solution occurs earlier than that in the 0.9 wt.% NaCl solution, indicating that the occurrence of localized corrosion in the 3.5 wt.% NaCl solution is much easier.

**Table 3.** The fitted EIS data on the basis of the equivalent circuits.

Conditions	$R_s$ ( $\Omega\text{ cm}^2$ )	$Y_{dl}$ ( $\mu\Omega^{-1}\text{cm}^{-2}\text{s}^n$ )	$n_{dl}$	$R_{ct}$ ( $\Omega\text{ cm}^2$ )	$Y_f$ ( $\mu\Omega^{-1}\text{cm}^{-2}\text{s}^n$ )	$n_f$	$R_f$ ( $\Omega\text{ cm}^2$ )	$L$ ( $\text{H cm}^{-2}$ )	$R_L$ ( $\Omega\text{ cm}^2$ )
In 0.9 wt.% NaCl	0 h								
	4 h	$24.2 \pm 0.5$	$20 \pm 2$	$0.91 \pm 0.03$	$1447 \pm 90$	$1537 \pm 150$	$738 \pm 75$	-	-
	8 h	$20.4 \pm 0.5$	$18 \pm 2$	$0.91 \pm 0.03$	$991 \pm 80$	$1245 \pm 125$	$521 \pm 65$	-	-
	24 h	$22.3 \pm 0.4$	$88 \pm 5$	$0.91 \pm 0.03$	$831 \pm 80$	-	-	$2619 \pm 348$	$175 \pm 58$
	h	$24.8 \pm 0.4$	$102 \pm 8$	$0.83 \pm 0.02$	$726 \pm 70$	-	-	$6840 \pm 465$	$382 \pm 95$
In 3.5 wt.% NaCl	0 h								
	4 h	$7.0 \pm 0.2$	$27 \pm 2$	$0.89 \pm 0.02$	$764 \pm 70$	$1829 \pm 176$	$394 \pm 35$	-	-
	8 h	$7.6 \pm 0.2$	$89 \pm 5$	$0.89 \pm 0.02$	$523 \pm 60$	-	-	$2185 \pm 315$	$146 \pm 54$
	24 h	$7.4 \pm 0.2$	$119 \pm 8$	$0.91 \pm 0.03$	$378 \pm 40$	-	-	$3695 \pm 385$	$204 \pm 69$
	h	$7.3 \pm 0.2$	$96 \pm 5$	$0.91 \pm 0.03$	$316 \pm 40$	-	-	$1482 \pm 175$	$111 \pm 45$

### 3.3. Hydrogen Evolution

Since the cathodic process of electrochemical corrosion of Mg alloys is due to the hydrogen evolution reaction, their corrosion rate can be calculated by the volume fraction of evolved hydrogen per unit of exposed area. Figure 6 shows the hydrogen evolution curves of the samples immersed in two concentrated NaCl solutions for up to 48 h. It reveals

that after immersion for 48 h, the hydrogen evolution volumes of the samples immersed in 0.9 wt.% and 3.5 wt.% NaCl solutions are 1.16 and 2.69 mL/cm<sup>2</sup>, respectively, indicating that the corrosion rate of the sample in the 3.5 wt.% NaCl solution is faster than that in the 0.9 wt.% solution. This result is consistent with the electrochemical measurements. Moreover, the variations of hydrogen evolution rates of the samples measured in the two concentrated solutions are different during the immersion process. When the immersion time is less than 8 h, the hydrogen evolution rates of the samples measured in the two concentrated solutions are low and their difference is quite small. When the immersion time exceeds 8 h, the hydrogen evolution rates of the samples immersed in the two concentrated solutions increase remarkably. Based on the slopes of hydrogen evolution curves, the hydrogen evolution rate of the alloy in the 3.5 wt.% NaCl solution is 3 times higher than that in the 0.9 wt.% NaCl solution.

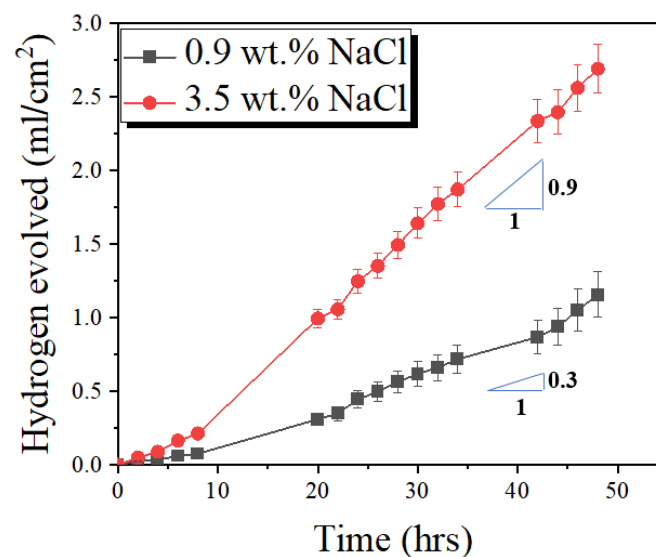


**Figure 6.** Hydrogen evolution curves of samples immersed in 0.9 wt.% NaCl and 3.5 wt.% NaCl solutions.

### 3.4. Observations to the Corrosion Morphologies

To reveal the different corrosion mechanisms of samples immersed in the two concentrated NaCl solutions, their surface corrosion morphologies and 3D images were observed and compared, as shown in Figures 7 and 8, respectively. At the early stage of corrosion, obvious filiform-like corrosion occurs on the surfaces of the different samples. Moreover, the corrosion severity of the samples in the two solutions intensifies with the prolongation of immersion time. When the immersion time is 4 h, the corrosion severity of the sample immersed in the 0.9 wt.% NaCl solution is significantly slighter than that in the 3.5 wt.% NaCl solution (Figures 7a and 8a). Based on the measured results from 3D images, the maximum depths of corrosion pits in the 0.9 wt.% and 3.5 wt.% NaCl solutions are 6.65  $\mu\text{m}$  and 14.07  $\mu\text{m}$ , respectively. Since a dense layer of  $\text{Li}_2\text{CO}_3$  can be formed on the surface of the  $\beta$ -Li phase [3,5,29–31], the subsequent corrosion attack to the substrate can be effectively inhibited. For the sample that is immersed in the 3.5 wt.% NaCl solution, the corrosion attack is much more severe and occurs widely in the  $\alpha$ -Mg phase. Moreover, the corrosion severity increases, and the depths of the corrosion pits become deeper when the immersion time increases. It is well known that the head of the filiform tip has the stronger acidity and can accelerate the corrosion, whilst the back of the filiform tip is alkaline and corrosion products are deposited [3]. When the immersion time is up to 24 h, some  $\beta$ -Li phases can still be present for the sample immersed in the 0.9 wt.% NaCl solution, whilst the whole surface of the sample that is immersed in the 3.5 wt.% NaCl solution is almost completely covered by the corrosion products. However, the maximum depths of the corrosion pits in the two solutions after immersion for 24 h are basically same and their values are 20.55  $\mu\text{m}$

and  $21.56\ \mu\text{m}$ , respectively. Combined with surface corrosion morphology and 3D images, it can be concluded that the corrosion attack of the Mg-8%Li alloy is much more severe in the 3.5 wt.% NaCl solution, which is consistent with the results of the hydrogen evolution and electrochemical tests.

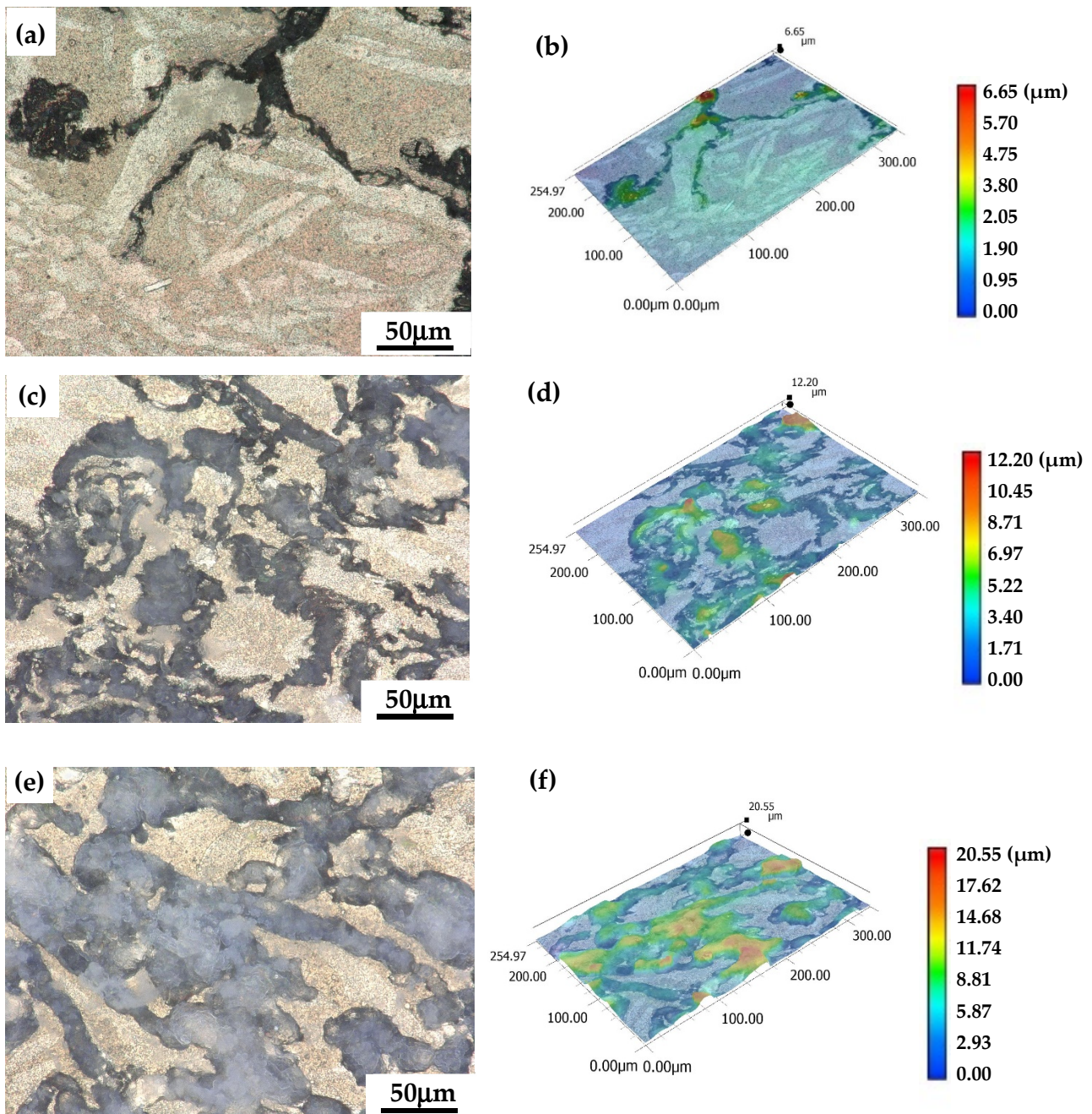


**Figure 7.** OM observations to the surface corrosion morphologies of the sample immersed in 0.9 wt.% solution for: (a) 4, (c) 8 and (e) 24 h. Images (b,d,f) are 3D profiles of surface corrosion morphologies of samples immersed in 3.5 wt.% solution for 4, 8 and 24 h.

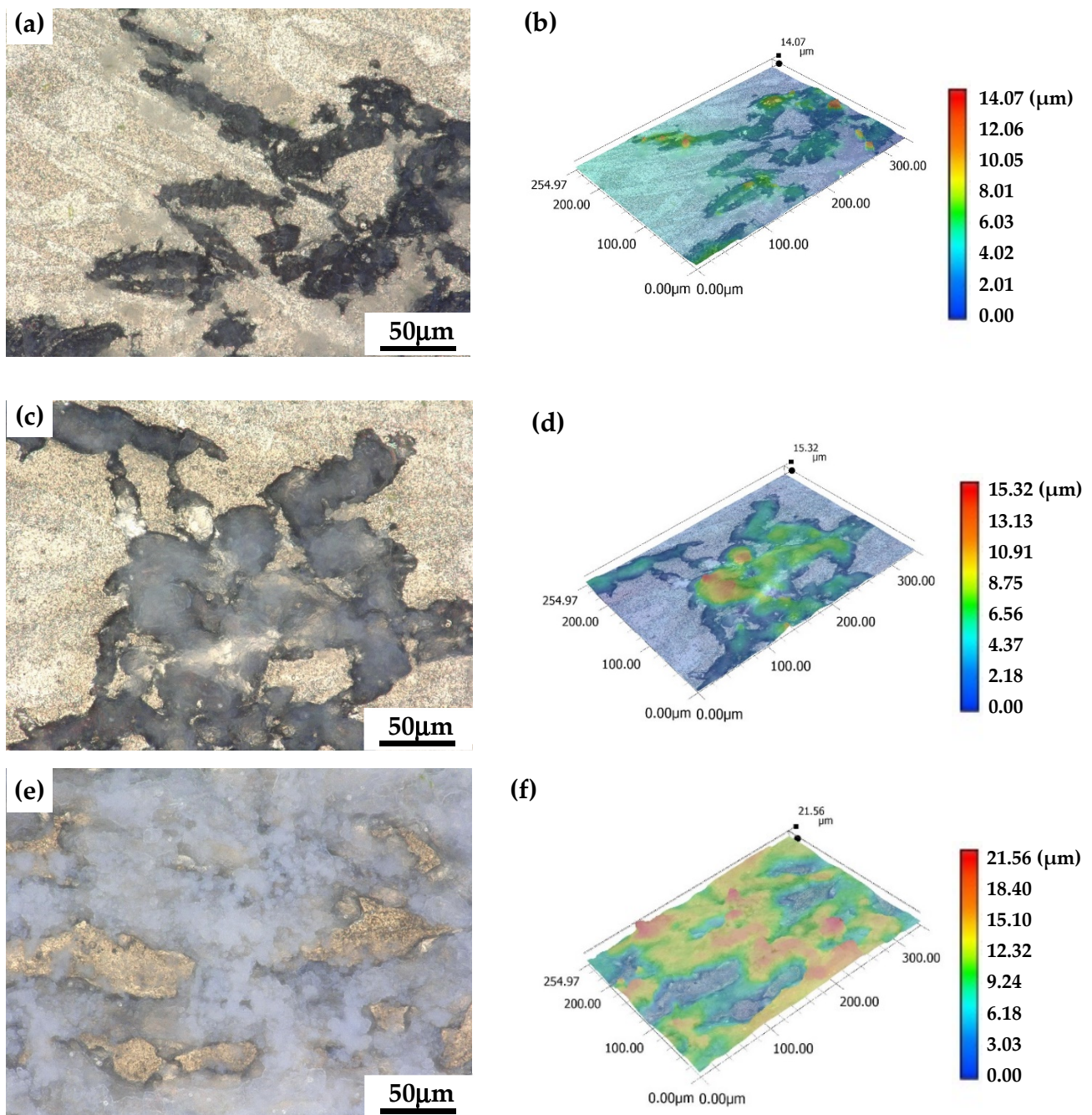


**Figure 8.** OM observations to the surface corrosion morphologies of the sample immersed in 3.5 wt.% solution for: (a) 4, (c) 8 and (e) 24 h. Images (b,d,f) are 3D profiles of surface corrosion morphologies of samples immersed in 3.5 wt.% solution for 4, 8 and 24 h.

Figure 9 shows the cross-sectional corrosion morphologies of the samples that are immersed in the two concentrated NaCl solutions for 4 h, respectively. It reveals that the localized corrosion attack of the sample immersed in the 3.5 wt.% NaCl is much more severe than that in the 0.9 wt.% NaCl (Figure 9a,b). Based on the high magnification images (Figure 9c), there are almost no visible corrosion pits on the surface. However, for the sample in 3.5 wt.% NaCl, the maximum depth of the corrosion pits can reach 10 μm (Figure 9b,d). Compared with the surface and cross-sectional observations, this indicates that although the filiform corrosion can easily occur on the surface of the Mg-8%Li alloy in differently concentrated NaCl solutions, the localized pitting is quite sensitive to the

concentration of  $\text{Cl}^-$ . High magnification images clearly show that the pitting can only occur in the 3.5 wt.% NaCl solution and preferentially nucleates in the interior of the  $\alpha$ -Mg matrix phases. Moreover, with the intensification of pitting corrosion, the electrolyte can reach underneath matrix and cause the dissolution of the  $\beta$ -Li phases because the  $\text{Li}_2\text{CO}_3$  film is hardly formed due to the limited concentration of  $\text{CO}_2$  in the solution, resulting in the corrosion of the whole surface of the sample that is immersed in the 3.5 wt.% NaCl solution for 24 h (Figure 8e). In a previous work, Song et al. reported that when the duplex structured Mg-8 wt.%Li alloy immersed in NaCl solution, the formed surface film was composed of MgO,  $\text{Li}_2\text{O}$ ,  $\text{Mg}(\text{OH})_2$  and LiOH [37]. Moreover, due to the reaction between  $\text{Li}_2\text{O}$  and  $\text{CO}_2$ , the  $\text{Li}_2\text{CO}_3$  can be formed on the surface of  $\beta$ -Li matrix phase. Generally, the Pilling–Bedworth ratio (PBR) of the formed film is between 1 and 2 [29]. It can have good protective capability for the underneath substrate. Zeng et al. reported that the PBR values of MgO,  $\text{Li}_2\text{O}$ ,  $\text{Mg}(\text{OH})_2$ , LiOH and  $\text{Li}_2\text{CO}_3$  are 0.88, 0.57, 1.77, 1.26 and 1.35, respectively [29]. In the previous work, Xu et al. reported that the formed  $\text{Li}_2\text{CO}_3$  film was dense and could protect the corrosion attack of the  $\beta$ -Li matrix phase, whereas the  $\text{MgCO}_3$  and  $\text{Mg}(\text{OH})_2$  films formed on the surface of  $\alpha$ -Mg phase were porous and loose [30]. Moreover, the  $\text{Cl}^-$  can easily destroy the  $\text{MgCO}_3$  and  $\text{Mg}(\text{OH})_2$  films formed on the surface of the  $\alpha$ -Mg phase [3]. Since the  $\text{Cl}^-$  concentration in the 3.5 wt.% NaCl solution is high, the stronger electrical conductivity of the solution can accelerate the electrochemical reactions and increase the corrosion rate of the alloy. Moreover, the high concentration of  $\text{Cl}^-$  can cause much more severe attacks to the surface films and reduce their corrosion protectiveness to the substrate. Thus, the difference of corrosion resistance of the alloys in the two concentrated NaCl solutions reaches the maximum when the immersion time is less than 4 h. With the increasing of the immersion time, the quantity of formed corrosion products on the sample surfaces will increase considerably. Then, the corrosion resistance due to the  $\text{Cl}^-$  attack can be offset by the increased corrosion products on the surfaces. This explains why the difference of corrosion resistance between the samples immersed in the 0.9 wt.% and 3.5 wt.% NaCl solutions decreases with the prolongation of immersion time. When the immersion time reaches 24 h, the corrosion severity on the surfaces of the differently immersed samples in the 0.9 wt.% and 3.5 NaCl solutions are basically the same (Figures 7f and 8f). Moreover, the initially localized corrosion increases the exposed area of the sample surfaces. Thus, when the immersion time exceeds 8 h, the hydrogen evolution rates of the samples immersed in the two concentrated NaCl solutions increase slightly.

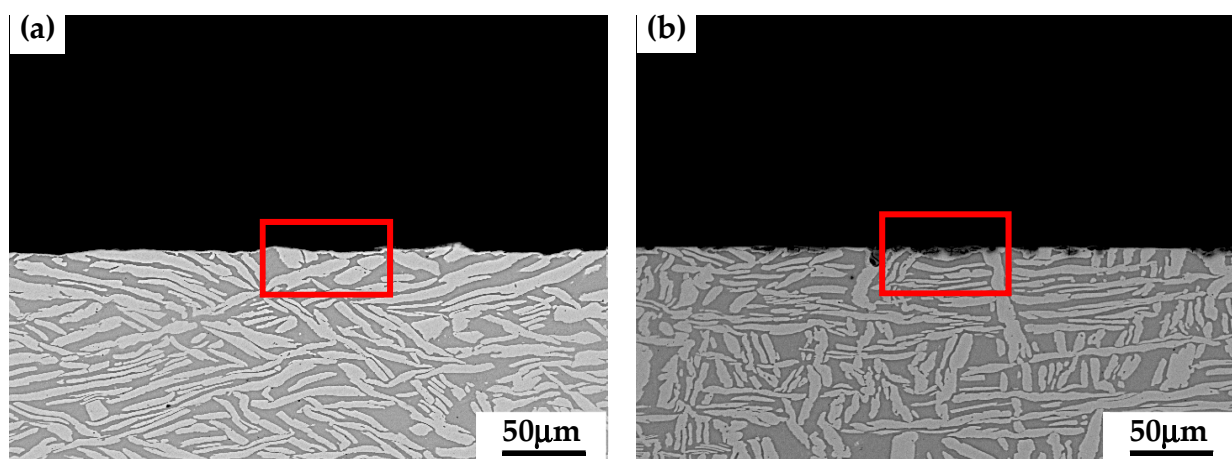
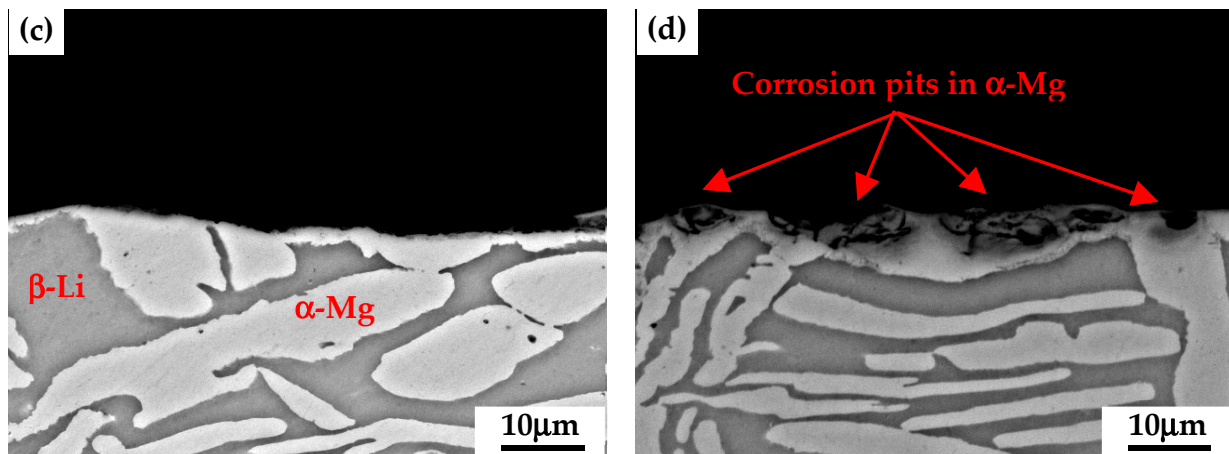


Figure 9. Cont.



**Figure 9.** SEM observations to the cross-sectional morphologies of the immersed samples in solutions of: (a) 0.9 wt.% and (b) 3.5 wt.% NaCl solutions for 4 h, respectively. Images (c,d) are high magnification observations to the areas squared in images (a,b), respectively.

#### 4. Conclusions

Through investigating and comparing the corrosion behavior of an as-rolled Mg-8%Li alloy in differently concentrated NaCl solutions, two conclusions can be drawn:

- (1) Based on the determined slopes of the measured hydrogen evolution curves, the corrosion rate of the alloy in the 3.5 wt.% NaCl solution is 3 times higher than that in the 0.9 wt.% NaCl solution when the immersion time exceeds 8 h.
- (2) The corrosion mechanisms of the as-rolled Mg-8%Li alloy are obviously different in the two concentrated NaCl solutions. In the 0.9 wt.% NaCl solution, the corrosion attack mainly occurs at the  $\alpha$ -Mg phase. In the 3.5 wt.% NaCl solution, the corrosion attack initially occurs in the  $\alpha$ -Mg phase and then gradually extends to the  $\beta$ -Li phase.

**Author Contributions:** Conceptualization, D.X. and B.W.; methodology, J.H.; software, J.L.; validation, B.W., H.S. and J.S.; formal analysis, B.W.; investigation, J.H.; resources, B.W.; data curation, H.S.; writing—original draft preparation, J.H.; writing—review and editing, J.S.; visualization, D.X. and B.W.; supervision, D.X.; project administration, D.X. and B.W.; funding acquisition, D.X. All authors have read and agreed to the published version of the manuscript.

**Funding:** This work was supported by the National Natural Science Foundation of China Projects under Grant [Nos. 52071220, 51871211, U21A2049, 51701129 and 51971054], Liaoning Province's project of "Revitalizing Liaoning Talents" (XLYC1907062), the Doctor Startup Fund of Natural Science Foundation Program of Liaoning Province (No. 2019-BS-200), High level achievement construction project of Shenyang Ligong University (SYLUXM202105), Liaoning BaiQianWan Talents Program, the Domain Foundation of Equipment Advance Research of 13th Five-year Plan (61409220118), National Key Research and Development Program of China under Grant [Nos. 2017YFB0702001 and 2016YFB0301105], the Innovation Fund of Institute of Metal Research (IMR), Chinese Academy of Sciences (CAS), the National Basic Research Program of China (973 Program) project under Grant No. 2013CB632205, and the Fundamental Research Fund for the Central Universities under Grant [No. N2009006].

**Institutional Review Board Statement:** Not applicable.

**Informed Consent Statement:** Not applicable.

**Data Availability Statement:** Not applicable.

**Conflicts of Interest:** The authors declare no conflict of interest.

## References

1. Zhu, W.H.; Zheng, Z.X.; Feng, J.Z.; Xu, H.H.; Wang, Y.T.; Lu, L.L. Dynamic Design Method for Magnesium Alloys Wheel of New Energy Vehicles. *Adv. Mater. Res.* **2010**, *961*, 930–934. [\[CrossRef\]](#)
2. Kannan, M.B.; Raman, P.K.S. In vitro degradation and mechanical integrity of calcium-containing magnesium alloys in modified-simulated body fluid. *Biomaterials* **2008**, *29*, 2306–2314. [\[CrossRef\]](#)
3. Wang, B.J.; Xu, D.K.; Cai, X.; Qiao, Y.X.; Sheng, L.Y. Effect of rolling ratios on the microstructural evolution and corrosion performance of an as-rolled Mg-8 wt.%Li alloy. *J. Magnes. Alloy.* **2021**, *9*, 560–568. [\[CrossRef\]](#)
4. Zhang, Y.; Xu, J.; Ruan, Y.C.; Yu, M.K.; O’Laughlin, M.; Wise, H.; Chen, D.; Tian, L.; Shi, D.; Wang, J.; et al. Implant-derived magnesium induces local neuronal production of CGRP to improve bone-fracture healing in rats. *Nat. Med.* **2016**, *22*, 1160–1169. [\[CrossRef\]](#)
5. Wang, B.J.; Xu, K.; Xu, D.K.; Cai, X.; Qiao, Y.X.; Sheng, L.Y. Anisotropic corrosion behavior of hot-rolled Mg-8 wt.%Li alloy. *J. Mater. Sci. Technol.* **2020**, *53*, 102–111. [\[CrossRef\]](#)
6. Tang, Q.B.; Huang, S.D.; Wu, T.B. Application analysis of magnesium alloys in weapon components. *Ordinance. Mater. Sci. Eng.* **2007**, *30*, 69–72.
7. Lv, Y.; Wang, L.; Li, Y.; Jin, Y.; Feng, J.; Ren, Y.M.; Cao, D.; Wang, G.; Zhang, M. The effect of different concentrations of Na<sub>2</sub>SnO<sub>3</sub> on the electrochemical behaviors of the Mg-8Li electrode. *Ionics* **2014**, *20*, 1573–1578. [\[CrossRef\]](#)
8. Chen, Z. *Magnesium Alloy*; Chemical Industry Press: Beijing, China, 2004.
9. Li, M.; Hao, H.; Zhang, A.; Song, Y.; Zhang, X. Effects of Nd on microstructure and mechanical properties of as-cast Mg-8Li-3Al alloy. *J. Rare Earths* **2012**, *30*, 492–496. [\[CrossRef\]](#)
10. Xu, D.K.; Li, C.Q.; Wang, B.J.; Han, E.H. Effect of icosahedral phase on the crystallographic texture and mechanical anisotropy of duplex structured Mg-Li alloys. *Mater. Des.* **2015**, *88*, 88–97. [\[CrossRef\]](#)
11. Xu, D.; Wang, B.; Li, C.; Zu, T.; Han, E. Effect of icosahedral phase on the thermal stability and ageing response of a duplex structured Mg-Li alloy. *Mater. Des.* **2015**, *69*, 124–129. [\[CrossRef\]](#)
12. Li, C.Q.; Xu, D.K.; Wang, B.J.; Sheng, L.Y.; Qiao, Y.X.; Han, E.H. Natural ageing responses of duplex structured Mg-Li based alloys. *Sci. Rep.* **2017**, *7*, 40078. [\[CrossRef\]](#)
13. Lv, Y.Z.; Xu, Y.; Wang, X.X.; Tian, H.L. The Electrochemical Performances of Mg-8Li, Mg-8Li-0.5Ce and Mg-8Li-1Ce Alloys in 0.7 mol·L<sup>-1</sup> NaCl Solution. *Acta. Chim. Sinica* **2011**, *69*, 2248–2252.
14. Xu, D.K.; Han, E.H. Effect of quasicrystalline phase on improving the corrosion resistance of a duplex structured Mg-Li alloy. *Scr. Mater.* **2014**, *71*, 21–24. [\[CrossRef\]](#)
15. Yang, L.H.; Jiang, Q.T.; Zheng, M.; Hou, B.; Li, Y. Corrosion behavior of Mg-8Li-3Zn-Al alloy in neutral 3.5% NaCl solution. *J. Magnes. Alloy* **2016**, *4*, 22–26. [\[CrossRef\]](#)
16. Yuan, X.; Yu, D.; Gao, L.-L.; Gao, H. Effect of Phosphate-Buffered Solution Corrosion on the Ratcheting Fatigue Behavior of a Duplex Mg-Li-Al Alloy. *J. Mater. Eng. Perform* **2016**, *25*, 1802–1810. [\[CrossRef\]](#)
17. Dobkowska, A.; Adamczyk-Cieslak, B.; Mizera, J.; Kubásek, J.; Vojtěch, D. Corrosion Behaviour of Magnesium Lithium Alloys in NaCl Solution. *Solid. State. Phenom.* **2015**, *3763*, 87–90. [\[CrossRef\]](#)
18. Thirumalaikumarasamy, D.; Shanmugam, K.; Balasubramanian, V. Comparison of the corrosion behaviour of AZ31B magnesium alloy under immersion test and potentiodynamic polarization test in NaCl solution. *J. Magnes. Alloy.* **2014**, *2*, 36–49. [\[CrossRef\]](#)
19. Shan, D.Y.; Zhou, W.Q.; Han, E.H.; Ke, W. Corrosion and electrochemical behavior of AZ31D magnesium alloys in sodium chloride. *Trans. Nonferr. Met. Soc. China* **2006**, *16*, 1789–1792.
20. Thirumalaikumarasamy, D.; Shanmugam, K.; Balasubramanian, V. Influence of chloride ion concentration on immersion corrosion behaviour of plasma sprayed alumina coatings on AZ31B magnesium alloy. *J. Magnes. Alloy.* **2014**, *2*, 325–334. [\[CrossRef\]](#)
21. Liu, F.; Song, Y.W.; Shan, D.Y.; Han, E.H. Corrosion behavior of AZ31 magnesium alloy in simulated acid rain solution. *Trans. Nonferrous Met. Soc. China* **2010**, *20*, 638–642. [\[CrossRef\]](#)
22. Li, M.M.; Qin, Z.; Yang, Y.; Xiong, X.M.; Zhou, G.; Cui, X.F.; Jiang, B.; Peng, X.D.; Pan, F.S. Microstructure and Corrosion Properties of Duplex-Structured Extruded Mg-6Li-4Zn-xMn Alloys. *Acta. Metall. Sin.* **2022**. [\[CrossRef\]](#)
23. Ma, X.C.; Jin, S.Y.; Wu, R.Z.; Wang, J.X.; Wang, G.X.; Krit, B.; Betsofen, S. Corrosion behavior of Mg-Li alloys: A review. *Trans. Nonferrous Met. Soc. China* **2021**, *31*, 3228–3254. [\[CrossRef\]](#)
24. Li, C.Q.; Liu, X.; Dong, L.J.; Shi, B.Q.; Tang, S.; Dong, Y.; Zhang, Z.R. Simultaneously improved mechanical strength and corrosion resistance of Mg-Li-Al alloy by solid solution treatment. *Mater. Lett.* **2021**, *301*, 130305. [\[CrossRef\]](#)
25. Dong, L.J.; Liu, X.; Liang, J.X.; Li, C.Q.; Dong, Y.; Zhang, Z.R. Corrosion behavior of a eutectic Mg-8Li alloy in NaCl solution. *Electrochem. Commun.* **2021**, *129*, 107087. [\[CrossRef\]](#)
26. Dobkowska, A.; Adamczyk-Cieslak, B.; Kubasek, J.; Vojtech, D.; Kuc, D.; Hadasik, E.; Mizera, J. Microstructure and corrosion resistance of a duplex structured Mg-7.5Li-3Al-1Zn. *J. Magnes. Alloy.* **2021**, *9*, 467–477. [\[CrossRef\]](#)
27. Li, C.Q.; He, Y.B.; Huang, H.P. Effect of lithium content on the mechanical and corrosion behaviors of HCP binary Mg-Li alloys. *J. Magnes. Alloy.* **2021**, *9*, 569–580. [\[CrossRef\]](#)
28. Wang, B.J.; Xu, D.K.; Sun, J.; Han, E.H. Effect of grain structure on the stress corrosion cracking (SCC) behavior of an as-extruded Mg-Zn-Zr alloy. *Corros. Sci.* **2019**, *157*, 347–356. [\[CrossRef\]](#)

29. Zeng, R.C.; Sun, L.; Zheng, Y.F.; Cui, H.Z.; Han, E.H. Corrosion and characterization of dual phase Mg-Li-Ca alloy in Hank's solution: The influence of microstructural features. *Corros. Sci.* **2014**, *79*, 69–82. [[CrossRef](#)]
30. Xu, W.; Birbilis, N.; Sha, G.; Wang, Y.; Daniels, J.; Xiao, Y.; Ferry, M. A high-specific-strength and corrosion-resistant magnesium alloy. *Nat. Mater.* **2015**, *14*, 1229–1235. [[CrossRef](#)]
31. Liu, G.; Xie, W.; Wei, G.; Yang, Y.; Liu, J.; Xu, T.; Xie, W.; Peng, X. Dynamic Recrystallization Behavior and Corrosion Resistance of a Dual-Phase Mg-Li Alloy. *Materials* **2018**, *11*, 408. [[CrossRef](#)]
32. Xin, Y.C.; Chu, P.K. Influence of Tris in simulated body fluid on degradation behavior of pure magnesium. *Mater. Chem. Phys.* **2010**, *124*, 33–35. [[CrossRef](#)]
33. Wang, B.J.; Xu, D.K.; Zhao, T.Y.; Sheng, L.Y. Effect of  $\text{CaCl}_2$  and  $\text{NaHCO}_3$  in physiological saline solution on the corrosion behavior of an as-extruded Mg-Zn-Y-Nd alloy. *Acta Metall. Sin.* **2021**, *34*, 239–247. [[CrossRef](#)]
34. Masing, G.; Tamman, G. Behavior of lithium, toward sodium, potassium, yin, cadmium and magnesium. *Z. Fur Anorg. Allg. Chem.* **1960**, *67*, 197–198.
35. Wang, B.J.; Xu, D.K.; Dong, J.H.; Ke, W. Effect of corrosion product films on the in vitro degradation behavior of Mg-3%Al-1%Zn (in wt%) alloy in Hank's solution. *J. Mater. Sci. Technol.* **2018**, *34*, 1756–1764. [[CrossRef](#)]
36. Li, C.Q.; Xu, D.K.; Chen, X.B.; Wang, B.J.; Wu, R.Z.; Han, E.H.; Birbilis, N. Composition and microstructure dependent corrosion behaviour of Mg-Li alloys. *Electrochim. Acta* **2018**, *260*, 55–64. [[CrossRef](#)]
37. Song, Y.W.; Shan, D.Y.; Chen, R.S.; Han, E.H. Investigation of surface oxide film on magnesium lithium alloy. *J. Alloys Compd.* **2009**, *484*, 585–590. [[CrossRef](#)]